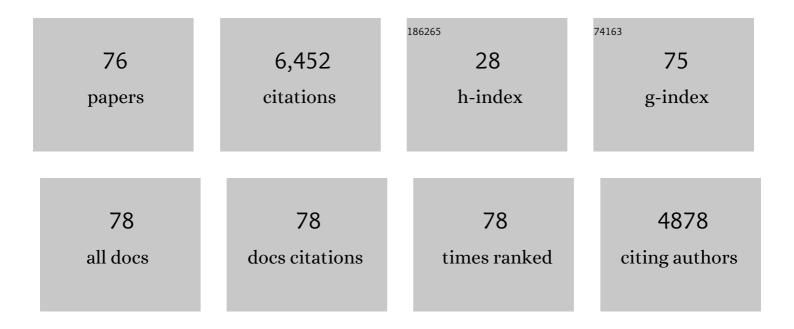
Greg Balco

List of Publications by Year in descending order

Source: https://exaly.com/author-pdf/11182046/publications.pdf Version: 2024-02-01



CREC RALCO

#	Article	IF	CITATIONS
1	A complete and easily accessible means of calculating surface exposure ages or erosion rates from 10Be and 26Al measurements. Quaternary Geochronology, 2008, 3, 174-195.	1.4	1,613
2	Joint determination of 40K decay constants and 40Arâ^—/40K for the Fish Canyon sanidine standard, and improved accuracy for 40Ar/39Ar geochronology. Geochimica Et Cosmochimica Acta, 2010, 74, 5349-5367.	3.9	717
3	Response to the comment by W.H. Schwarz et al. on "Joint determination of 40K decay constants and 40Arâ^—/40K for the Fish Canyon sanidine standard, and improved accuracy for 40Ar/39Ar geochronology―by P.R. Renne et al. (2010). Geochimica Et Cosmochimica Acta, 2011, 75, 5097-5100.	3.9	542
4	Geological calibration of spallation production rates in the CRONUS-Earth project. Quaternary Geochronology, 2016, 31, 188-198.	1.4	503
5	Regional beryllium-10 production rate calibration for late-glacial northeastern North America. Quaternary Geochronology, 2009, 4, 93-107.	1.4	323
6	Contributions and unrealized potential contributions of cosmogenic-nuclide exposure dating to glacier chronology, 1990–2010. Quaternary Science Reviews, 2011, 30, 3-27.	3.0	307
7	Cosmogenic nuclide systematics and the CRONUScalc program. Quaternary Geochronology, 2016, 31, 160-187.	1.4	246
8	The CRONUS-Earth Project: A synthesis. Quaternary Geochronology, 2016, 31, 119-154.	1.4	138
9	Absolute chronology for major Pleistocene advances of the Laurentide Ice Sheet. Geology, 2010, 38, 795-798.	4.4	136
10	Production rate calculations for cosmic-ray-muon-produced 10Be and 26Al benchmarked against geological calibration data. Quaternary Geochronology, 2017, 39, 150-173.	1.4	121
11	Selective glacial erosion and weathering zones in the coastal mountains of Marie Byrd Land, Antarctica. Geomorphology, 2005, 67, 317-334.	2.6	108
12	A reevaluation of in situ cosmogenic 3He production rates. Quaternary Geochronology, 2010, 5, 410-418.	1.4	105
13	Greenland was nearly ice-free for extended periods during the Pleistocene. Nature, 2016, 540, 252-255.	27.8	95
14	Thermochronometry Reveals Headward Propagation of Erosion in an Alpine Landscape. Science, 2011, 332, 84-88.	12.6	90
15	The First Glacial Maximum in North America. Science, 2005, 307, 222-222.	12.6	88
16	Production rate of cosmogenic 21Ne in quartz estimated from 10Be, 26Al, and 21Ne concentrations in slowly eroding Antarctic bedrock surfaces. Earth and Planetary Science Letters, 2009, 281, 48-58.	4.4	74
17	Cosmogenic-nuclide ages for New England coastal moraines, Martha's Vineyard and Cape Cod, Massachusetts, USA. Quaternary Science Reviews, 2002, 21, 2127-2135.	3.0	68
18	26Al–10Be–21Ne burial dating. Earth and Planetary Science Letters, 2009, 286, 570-575.	4.4	68

GREG BALCO

#	Article	IF	CITATIONS
19	Canyon incision and knickpoint propagation recorded by apatite 4He/3He thermochronometry. Earth and Planetary Science Letters, 2010, 293, 377-387.	4.4	61
20	Cosmogenic 3He in hematite and goethite from Brazilian "canga―duricrust demonstrates the extreme stability of these surfaces. Earth and Planetary Science Letters, 2012, 329-330, 41-50.	4.4	60
21	Glacier Change and Paleoclimate Applications of Cosmogenic-Nuclide Exposure Dating. Annual Review of Earth and Planetary Sciences, 2020, 48, 21-48.	11.0	59
22	Cosmogenic-nuclide burial ages for Pleistocene sedimentary fill in Unaweep Canyon, Colorado, USA. Quaternary Geochronology, 2013, 18, 149-157.	1.4	54
23	A record of impacts preserved in the lunar regolith. Earth and Planetary Science Letters, 2010, 290, 155-165.	4.4	51
24	Exposure-age record of Holocene ice sheet and ice shelf change in the northeast Antarctic Peninsula. Quaternary Science Reviews, 2013, 59, 101-111.	3.0	45
25	Interlaboratory comparison of cosmogenic 21 Ne in quartz. Quaternary Geochronology, 2015, 26, 20-28.	1.4	44
26	Numerical ages for Plio-Pleistocene glacial sediment sequences by 26Al/10Be dating of quartz in buried paleosols. Earth and Planetary Science Letters, 2005, 232, 179-191.	4.4	40
27	Measuring middle Pleistocene erosion rates with cosmic-ray-produced nuclides in buried alluvial sediment, Fisher Valley, southeastern Utah. Earth Surface Processes and Landforms, 2005, 30, 1051-1067.	2.5	34
28	Active erosion–deposition cycles in the hyperarid Atacama Desert of Northern Chile. Earth and Planetary Science Letters, 2013, 371-372, 125-133.	4.4	32
29	Slow regolith degradation without creep determined by cosmogenic nuclide measurements in Arena Valley, Antarctica. Quaternary Research, 2008, 69, 242-249.	1.7	28
30	Exposure dating of precariously balanced rocks. Quaternary Geochronology, 2011, 6, 295-303.	1.4	27
31	Basins and bedrock: Spatial variation in 10Be erosion rates and increasing relief in the southern Rocky Mountains, USA. Geology, 2014, 42, 167-170.	4.4	27
32	Features of the glacial history of the Transantarctic Mountains inferred from cosmogenic ²⁶ Al, ¹⁰ Be and ²¹ Ne concentrations in bedrock surfaces. Antarctic Science, 2014, 26, 708-723.	0.9	27
33	Diffusion kinetics of 3 He and 21 Ne in quartz and implications for cosmogenic noble gas paleothermometry. Geochimica Et Cosmochimica Acta, 2014, 142, 186-204.	3.9	26
34	Cosmogenic noble gas paleothermometry. Earth and Planetary Science Letters, 2014, 400, 195-205.	4.4	25
35	Late-glacial grounding line retreat in the northern Ross Sea, Antarctica. Geology, 2019, 47, 291-294.	4.4	25
36	A 14.5-million-year record of East Antarctic Ice Sheet fluctuations from the central Transantarctic Mountains, constrained with cosmogenic ³ He, ¹⁰ Be, ²¹ Ne, and ²⁶ Al. Cryosphere, 2020, 14, 2647-2672.	3.9	25

GREG BALCO

#	Article	IF	CITATIONS
37	New Last Glacial Maximum ice thickness constraints for the Weddell Sea Embayment, Antarctica. Cryosphere, 2019, 13, 2935-2951.	3.9	24
38	Rate of fluvial incision in the Central Alps constrained through joint inversion of detrital 10Be and thermochronometric data. Earth and Planetary Science Letters, 2015, 411, 27-36.	4.4	23
39	Degradation of glacial deposits quantified with cosmogenic nuclides, Quartermain Mountains, Antarctica. Earth Surface Processes and Landforms, 2011, 36, 217-228.	2.5	22
40	Late Quaternary deglacial history across the Larsen B embayment, Antarctica. Quaternary Science Reviews, 2018, 189, 134-148.	3.0	22
41	Million year old ice found under meter thick debris layer in Antarctica. Geophysical Research Letters, 2016, 43, 6995-7001.	4.0	20
42	Abrupt mid-Holocene ice loss in the western Weddell Sea Embayment of Antarctica. Earth and Planetary Science Letters, 2019, 518, 127-135.	4.4	20
43	Technical note: A prototype transparent-middle-layer data management and analysis infrastructure for cosmogenic-nuclide exposure dating. Geochronology, 2020, 2, 169-175.	2.5	20
44	Neon diffusion kinetics in olivine, pyroxene and feldspar: Retentivity of cosmogenic and nucleogenic neon. Geochimica Et Cosmochimica Acta, 2012, 86, 21-36.	3.9	17
45	Review article: Existing and potential evidence for Holocene grounding line retreat and readvance in Antarctica. Cryosphere, 2022, 16, 1543-1562.	3.9	16
46	Simple computer code for estimating cosmic-ray shielding by oddly shaped objects. Quaternary Geochronology, 2014, 22, 175-182.	1.4	15
47	Deglaciation and late-glacial climate change in the White Mountains, New Hampshire, USA. Quaternary Research, 2017, 87, 96-120.	1.7	15
48	Cosmogenic and nucleogenic 21Ne in quartz in a 28-meter sandstone core from the McMurdo Dry Valleys, Antarctica. Quaternary Geochronology, 2019, 52, 63-76.	1.4	15
49	Quantifying regolith erosion rates with cosmogenic nuclides ¹⁰ Be and ²⁶ Al in the McMurdo Dry Valleys, Antarctica. Journal of Geophysical Research, 2010, 115, .	3.3	13
50	Radar-detected englacial stratigraphy in the Pensacola Mountains, Antarctica: implications for recent changes in ice flow and accumulation. Annals of Glaciology, 2013, 54, 91-100.	1.4	13
51	Exposure-age data from across Antarctica reveal mid-Miocene establishment of polar desert climate. Geology, 2021, 49, 91-95.	4.4	12
52	Relative sea-level data preclude major late Holocene ice-mass change in Pine Island Bay. Nature Geoscience, 2022, 15, 568-572.	12.9	12
53	The Geographic Footprint of Glacier Change. Science, 2009, 324, 599-600.	12.6	10
54	Periglacial Climate at the 2.5 Ma Onset of Northern Hemisphere Glaciation Inferred from the Whippoorwill Formation, Northern Missouri, USA. Quaternary Research, 2010, 73, 151-161.	1.7	10

Greg Balco

#	Article	IF	CITATIONS
55	Geology of Unaweep Canyon and its role in the drainage evolution of the northern Colorado Plateau. , 2015, 11, 320-341.		10
56	Paleoclimatic interpretations of buried paleosols within the pre-Illinoian till sequence in northern Missouri, USA. Palaeogeography, Palaeoclimatology, Palaeoecology, 2015, 417, 44-56.	2.3	10
57	Empirical Evidence for Latitude and Altitude Variation of the In Situ Cosmogenic 26Al/10Be Production Ratio. Geosciences (Switzerland), 2021, 11, 402.	2.2	10
58	Summary of Early and Middle Pleistocene Glaciations in Northern Missouri, USA. Developments in Quaternary Sciences, 2011, 15, 553-561.	0.1	9
59	Glacial geology and cosmogenic-nuclide exposure ages from the Tucker Glacier - Whitehall Glacier confluence, northern Victoria Land, Antarctica. Numerische Mathematik, 2019, 319, 255-286.	1.4	9
60	Detrital Thermochronometry Reveals That the Topography Along the Antarctic Peninsula is Not a Pleistocene Landscape. Journal of Geophysical Research F: Earth Surface, 2020, 125, e2019JF005447.	2.8	8
61	Mid-Holocene thinning of David Glacier, Antarctica: chronology and controls. Cryosphere, 2021, 15, 5447-5471.	3.9	8
62	Regolith transport quantified by braking block, McMurdo Dry Valleys, Antarctica. Geomorphology, 2012, 155-156, 80-87.	2.6	7
63	Glacial chronology and slip rate on the west Klamath Lake fault zone, Oregon. Bulletin of the Geological Society of America, 2019, 131, 444-460.	3.3	7
64	Performance of CRONUS-P – A pyroxene reference material for helium isotope analysis. Quaternary Geochronology, 2016, 31, 237-239.	1.4	6
65	Boulder weathering in McMurdo Dry Valleys, Antarctica. Geomorphology, 2014, 219, 192-199.	2.6	5
66	The absence of evidence of absence of the East Antarctic Ice Sheet. Geology, 2015, 43, 943-944.	4.4	5
67	Chlorine-36â^•beryllium-10 burial dating of alluvial fan sediments associated with the Mission Creek strand of the San Andreas Fault system, California, USA. Geochronology, 2019, 1, 1-16.	2.5	5
68	Cosmogenic nuclide dating of two stacked ice masses: Ong Valley, Antarctica. Cryosphere, 2022, 16, 2793-2817.	3.9	5
69	Early-to-mid Miocene erosion rates inferred from pre-Dead Sea rift Hazeva River fluvial chert pebbles using cosmogenic ²¹ Ne. Earth Surface Dynamics, 2020, 8, 289-301.	2.4	4
70	Neon diffusion kinetics and implications for cosmogenic neon paleothermometry in feldspars. Geochimica Et Cosmochimica Acta, 2017, 205, 14-30.	3.9	3
71	Cosmogenic nuclide and solute flux data from central Cuban rivers emphasize the importance of both physical and chemical mass loss from tropical landscapes. Geochronology, 2022, 4, 435-453.	2.5	3
72	Atmospherically produced beryllium-10 in annually laminated late-glacial sediments of the North American Varve Chronology. Geochronology, 2021, 3, 1-33.	2.5	2

Greg Balco

#	Article	IF	CITATIONS
73	Tectonic controls on the timing of fjord incision at the Antarctic Peninsula. Earth and Planetary Science Letters, 2022, 585, 117528.	4.4	2
74	Stratigraphy, paleomagnetism, and cosmogenic-isotope burial ages of fossil-bearing strata within Riverbluff Cave, Greene County, Missouri. Quaternary Research, 2017, 87, 516-528.	1.7	1
75	Miocene to Pleistocene glacial history of West Antarctica inferred from Nunatak geomorphology and cosmogenic-nuclide measurements on bedrock surfaces. Numerische Mathematik, 2020, 320, 637-676.	1.4	1
76	Improving West Antarctic ice sheet reconstructions from compiling local GPR observations. , 2020, , .		0